IEEE Photonics Journal
An IEEE Photonics Society Publication

A CMOS Compatible Ultracompact Silicon Photonic Optical Add-Drop Multiplexer with Misaligned Sidewall Bragg Gratings

Volume 9, Number 3, June 2017

Md Ghulam Saber
Zhenping Xing
David Patel
Eslam El-Fiky
Nicolás Abadía
Yun Wang
Maxime Jacques
M. Morsy-Osman
David V. Plant

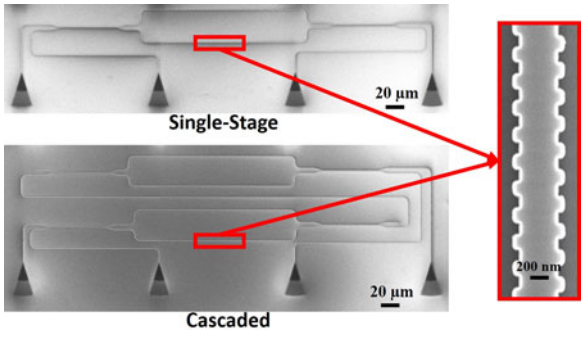

DOI: 10.1109/JPHOT.2017.2703857
1943-0655 © 2017 IEEE

IEEE photonics SOCIETY

IEEE

A CMOS Compatible Ultracompact Silicon Photonic Optical Add-Drop Multiplexer with Misaligned Sidewall Bragg Gratings

Md Ghulam Saber, Zhenping Xing, David Patel, Eslam El-Fiky, Nicolás Abadía, Yun Wang, Maxime Jacques, M. Morsy-Osman, and David V. Plant

Department of Electrical and Computer Engineering, McGill University, Montreal, QC H3A 0E9, Canada

DOI:10.1109/JPHOT.2017.2703857

Manuscript received March 21, 2017; revised May 6, 2017; accepted May 9, 2017. Date of publication May 12, 2017; date of current version May 31, 2017. The work of Md Ghulam Saber was supported in part by Fonds de Recherche-Nature et Technologies Québec (PBEEE V1 Dossier # 200755) and in part by RH Tomlinson Fellowship (90025) of McGill University. Corresponding author: Md Ghulam Saber (e-mail: md.saber@mail.mcgill.ca)

Abstract: We experimentally and via simulations demonstrate ultracompact single-stage and cascaded optical add-drop multiplexers using misaligned sidewall Bragg grating in a Mach–Zehnder interferometer for the silicon-on-insulator platform. The single-stage configuration has a device footprint of 400 μm $\times$ 90 μm, and the cascaded configuration has a footprint of 400 μm $\times$ 125 μm. The proposed designs have 3-dB bandwidths of 6 nm and extinction ratios of 25 dB and 51 dB, respectively, and have been fabricated for the transverse electric mode. A minimum lithographic feature size of 80 nm is used in our design, which is within the limitation of 193 nm deep ultraviolet lithography.

Index Terms: Optical add-drop multiplexer, misaligned Bragg grating, silicon-on-insulator, silicon photonics, integrated optics, optoelectronics.

1. Introduction

Silicon photonics is considered a key technology for next generation optical interconnects and communication systems due to its low power operation, scalability and compatibility with the complementary metal oxide semiconductor (CMOS) process [1], [2]. The silicon-on-insulator (SOI) platform has a large index contrast between the core and the cladding, thus allowing for nanoscale waveguides and denser integration of photonic components [1]. Silicon photonic devices are also being considered for wavelength-division multiplexing (WDM) metro and long haul network segments [3]–[6].

Optical add-drop multiplexers (OADMs) select and route WDM channels. Researchers have been developing OADMs in non-SOI platforms [7]–[11], and more recently in SOI platforms [12]–[18]. In the SOI platform, ring resonator [12]–[14], grating-assisted contra-directional coupler [16]–[18], and Bragg grating (BG) [15], [19] based devices have received much attention. Ring resonators are compact but achieving a flat-top spectral response, and a large free spectral range (FSR) is challenging. Grating-assisted contra-directional coupler based devices are complex in design and large extinction ratio (ER) is difficult to achieve [16], [18], [20]. BG based devices, on the other hand, offer FSR free operation and several degrees of freedom to achieve desired spectral response.

BGs are reflection-based devices and therefore, optical circulators are required in order to use them as multiplexers. Optical circulators are difficult to achieve in SOI since they require non-CMOS compatible materials [21]. Circulators are available as discrete optical components, but this increases packaging complexity [22]. One solution to this problem is to incorporate BGs in interferometric structures [23]. BGs in Mach-Zehnder interferometer (MZI) based OADM in SOI have been reported in the past by several groups. A Si-wire waveguide based BGs in MZI OADM with a 3-dB bandwidth (BW) of 0.7 nm was reported in [19]. But it has a very small ER of 8 dB and a relatively long length of 800 μm. In [15], two OADM configurations based on BGs in MZIs which offered a 3-dB BW of 3.5 nm and ERs of 40 dB and 45 dB were reported. However, the footprints were 391 μm $\times$ 1400 μm and 391 μm $\times$ 3600 μm, respectively, which are excessively large. Recently, a new technique to precisely control the coupling coefficient of silicon waveguide BGs by misaligning the sidewall gratings was reported in [24]. This technique significantly alleviates the problem of quantization error which occurs because of finite size of the mask grid [24]. In this paper, we propose ultra-compact OADMs in the C-band using misaligned sidewall gratings. We analyze two configurations of the BGs in MZI-based OADMs. We refer to the first design as a single-stage design and the second as a cascaded design. The effects of misalignment variation on the spectral response of both structures was studied numerically and experimentally. The use of misaligned gratings enables a narrow BW with a lower number of periods, thus enabling optimization of the OADM designs for compactness. We experimentally measured 3-dB BWs of 6 nm and 6.2 nm and ERs of 25 dB and 51 dB with device footprints of 400 μm $\times$ 90 μm and 400 μm $\times$ 125 μm, respectively for the single-stage and the cascaded configuration. This corresponds to 15 and 28 times smaller footprint than previously reported devices in [15]. An improvement of 3 dB and 4.5 dB in insertion losses of input-to-drop and input-to-through ports is achieved with respect to [15]. Furthermore, the OAMDs are designed with 193 nm deep ultraviolet lithography compatible minimum feature size.

2. Device Design and Simulations

The organization of this section is as follows. In Section 2.1 theory of misaligned sidewall grating is described. The principle of operation of the device is presented in Section 2.2 and finally in Section 2.3 the simulations results are discussed.

2.1 Misaligned Sidewall Gratings

The Bragg condition is given as [25]

$$\lambda_{Bragg} = 2n_{avg}\Lambda \tag{1}$$

where λ_{Bragg} is the Bragg wavelength, n_{avg} is the average effective refractive index of the whole grating structure and Λ is the grating period.

Silicon BGs are normally created by periodic corrugations in the side-wall of a silicon waveguide. Each period of the grating works as a weak reflector due to its index discontinuity. To satisfy the Bragg condition, the grating period, Λ has to be such that all partial reflections add up in phase. In a uniform BG where the refractive index varies as $n(z) = n_{avg} + \Delta n \cos(2\pi z/\Lambda)$ along the grating longitudinal axis, the grating amplitude reflection coefficient is given as [25]

$$r_g = \frac{i\zeta \sin(qL)}{q\cos(qL) - i\Delta\beta \sin(qL)} \tag{2}$$

where $\zeta = 2\pi\Delta n/\lambda$ is the coupling coefficient which is related to the refractive index modulation depth, $q = \sqrt{\Delta\beta^2 - \zeta^2}$, L is the grating length, $\Delta\beta = \beta - \beta_{Bragg}$ is the propagation constant deviation from the Bragg wavelength and $\beta_{Bragg} = \frac{2\pi n_{avg}}{\lambda_{Bragg}}$. From (2), it can be seen that the grating reflection spectrum depends on the refractive index modulation depth and the grating length. BGs with weak coupling strengths are required to achieve narrow BW which can be designed by reducing the the structural corrugation width. The BW is also inversely proportional to the length in such weak

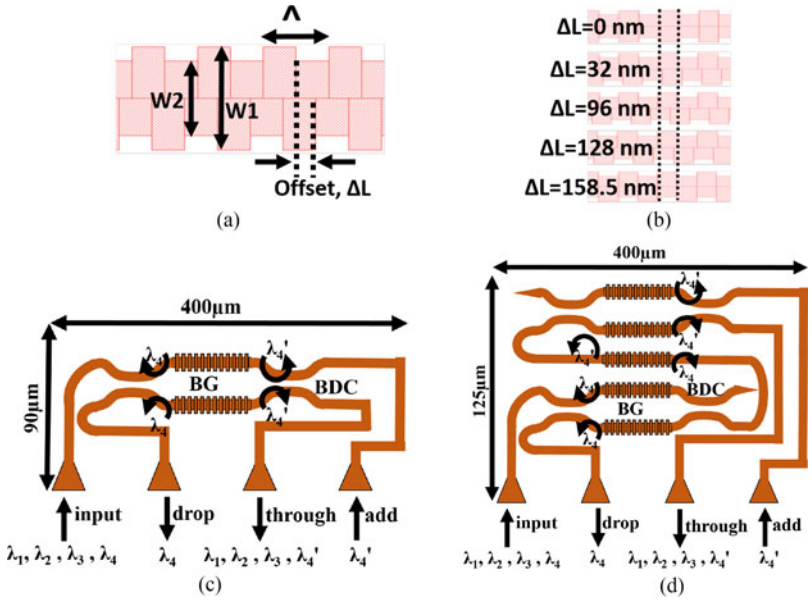

Fig. 1. (a) Misaligned sidewall Bragg grating, (b) variation of ΔL . Schematic of the fabricated (c) single-stage OADM configuration, (d) cascaded OADM configuration. Here, λ_4=λ_4'.

BGs [25]. Therefore, longer gratings are required to obtain narrow BW devices, which increases the device's footprint significantly. Since, achieving a narrow BW (e.g., 1 nm) requires a very small corrugation amplitude, the performance of the Bragg gratings become highly sensitive to variations in the fabrication processes. Wang *et al.* [24] proposed misaligning the sidewall gratings intentionally to control the grating coupling coefficient. The misaligned grating structure can be broken down into two separate gratings with a phase offset. The effective coupling coefficient of such a grating can be written as [24]

$$\kappa = \left| \frac{\kappa_0}{2} + \frac{\kappa_0}{2} \exp(i.2\pi\Delta L/\Lambda) \right| = \kappa_0 \cos\left(\frac{\pi\Delta L}{\Lambda}\right) \tag{3}$$

where κ_0 is the coupling coefficient when there is no misalignment, ΔL is the grating misalignment and $2\pi\Delta L/\Lambda$ is the phase offset. From (3), it can be seen that as the misalignment increases, reflections from each grating period interferes less constructively thus weakening the grating strength. Using this technique, narrow BW BGs can be created with a smaller number of grating periods. When the corrugations on the two sidewalls are completely misaligned, the grating periods interfere destructively, and the structure no longer reflects light. Moreover, this method of weakening the grating strength is less sensitive to fabrication quantization error than reducing the corrugation amplitude [24].

2.2 Principle of Operation

Fig. 1(a) depicts the Bragg grating corrugation parameters used in our design. Here, W1 was chosen to be 580 nm and W2 to be 420 nm. Therefore, the corrugation amplitude, ($\Delta W = \frac{W1-W2}{2}$) is 80 nm. The simulated effective refractive index of the 580 nm (n_{eff1}) and 420 nm (n_{eff2}) silicon waveguides as a function of wavelength are shown in Fig. 2. At 1542.5 nm wavelength, n_{eff1}=2.56 and n_{eff2}=2.29; thus, n_{avg}=2.43. From the Bragg condition in (1), Λ is found to be 317 nm. Fig. 1(b) shows the variation in the offset of the sidewall gratings starting from 0 nm to half of the grating period, i.e., 158.5 nm. At this offset, the two sidewalls are completely out of phase and the structure will not reflect light. The schematics of the two configurations of the OADMs, single-stage and cascaded, are shown in Fig. 1(c) and (d), respectively. All BGs have been designed to have the same Bragg wavelength. Both arms of the MZI have equal lengths and the BGs were placed

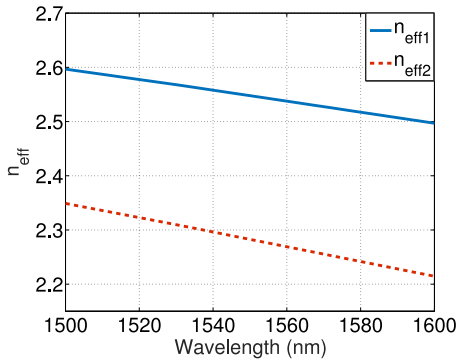

Fig. 2. Simulated effective refractive index of the 580 nm, n_{eff1} and 420 nm, n_{eff2} silicon waveguides as a function of wavelength.

symmetrically within each arm of the MZI. Broadband directional couplers (BDCs) [26] were used as 2×2 power splitter and combiner in the test structure.

Referring to Fig. 1(c), light consisting of several wavelengths is launched at the input port of the OADM. Since the BGs have a Bragg wavelength of λ_4, light at λ_4 will be reflected. The reflected light exits at the drop port because of the π phase shift induced by the directional coupler during a round trip. The other wavelengths which were outside the reflection BW of the BG will emerge at the through port, again because of the π phase shift caused by the directional coupler. Since the BGs in the MZI based OADMs are symmetric, light at λ_4 injected at the add port will get reflected by the BGs. The reflected light will exit via the through port, along with other wavelengths that were launched at the input port (except the dropped one).

Referring to Fig. 1(d), the cascaded design of the OADM has two identical single-stage OADMs with an additional BG in the connecting path. The open branches of the single-stage OADMs are terminated with optical terminators. The drop port of the cascaded configuration works on the same principle as the single-stage one. However, the additional BG in between the OADMs reflects residue light at λ_4 that was not reflected by the BGs in the first single-stage OADM and prevents it from emerging at the through port. Similarly, if light at λ_4 is launched at the add port, it will be reflected by the BGs in the second stage of the OADM and exit via the through port. The BG in between the OADMs will reflect any power that leaked through the second stage of the OADM at this wavelength so that it does not appear at the drop port. With the cascaded configuration, the ER of the OADM can be increased significantly and the cross-talk can be reduced. However, the improved ER and reduced crosstalk come at the expense of additional insertion loss and footprint.

2.3 Simulation Results

The OADM configurations were first simulated by varying ΔW, ΔL, and the number of grating periods, NG. All the simulations were done in *Lumerical Interconnect* [27] and the *Silicon Electronic-Photonic Integrated Circuits (Si-EPIC)* electron-beam process design kit was utilized [28]. The transmission graphs for the variation of ΔW are shown in Fig. 3(a) and (d), respectively for the single-stage and the cascaded configuration. It can be observed that the ER and BW increases as ΔW is increased. We varied ΔW up to 100 nm since a larger value of ΔW would increase the ER further which can not be measured physically. The lower value of ΔW was chosen based on the minimum fabricated feature size that has been reported in the literature. ΔL was varied from 0 nm to 158.5 nm (half the grating period) and the results are shown in Fig. 3(b) and (e), respectively for the single-stage and the cascaded configuration. The ER and BW exhibits a decreasing nature as ΔL is increased. The results for the variation of NG is provided in Fig. 3(c) and (f) for the single-stage and the cascaded configuration, respectively. The ER decreases but the BW remains constant if NG is decreased as can be seen from the figures. The upper value of NG was chosen because a higher value would increase the ER further which can not be measured physically. Furthermore, it

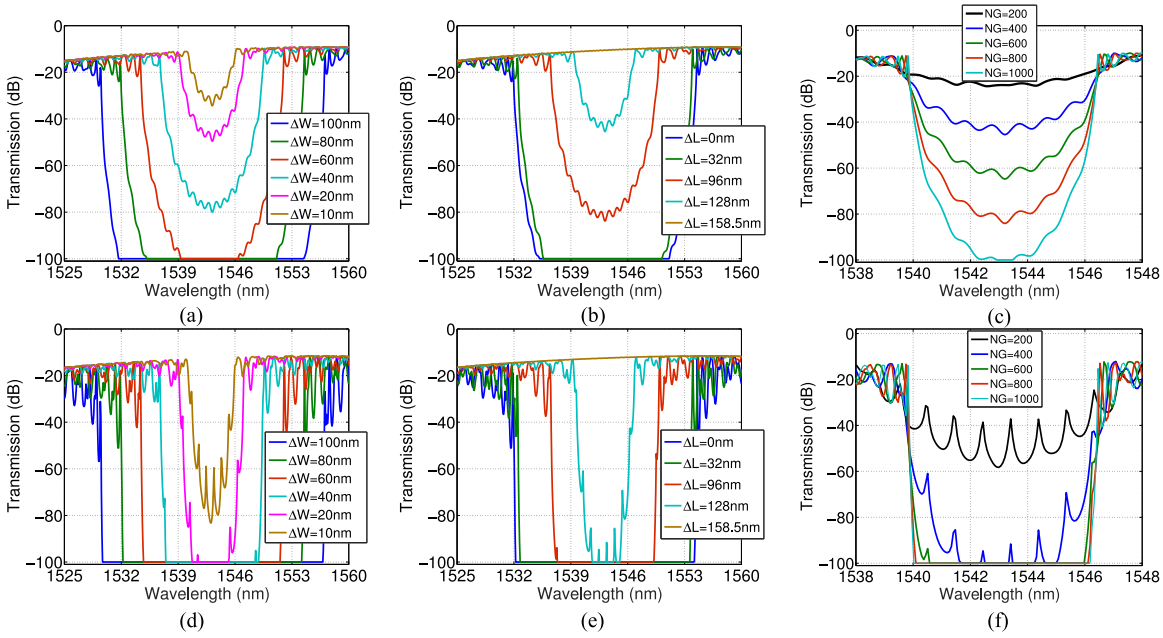

Fig. 3. Simulated transmission responses for the single-stage configuration for (a) different ΔW with NG $= 400$ and $\Delta L = 0$ nm, (b) different ΔL with $\Delta W = 80$ nm and NG $= 400$, and (c) different NG with $\Delta W = 80$ nm and $\Delta L = 128$ nm. Simulated transmission responses for the cascaded configuration for (d) different ΔW with NG $= 400$ and $\Delta L = 0$ nm, (e) different ΔL with $\Delta W = 80$ nm and NG $= 400$, and (f) different NG with $\Delta W = 80$ nm and $\Delta L = 128$ nm.

would increase the footprint and insertion loss of the device. The cascaded configuration achieves significantly larger ER for both ΔW and ΔL variation. The sensitivity of the power meter in the simulation software was set to -100 dB and is why clipping can be observed in Fig. 3. We chose this value for power meter sensitivity because a ER value of less than -100 dB cannot be measured physically. The clipping phenomenon indicates that the OADMs have higher ER than what we can observe.

From the results presented in Fig. 3, we will choose ΔW, ΔL, and NG by balancing ER, BW and device compactness. For NG $= 200$, the ERs are only 12 dB and 26 dB for the single-stage and the cascaded configuration, respectively whereas for NG $= 400$, the ERs are 35.5 dB and 85.85 dB, respectively. Since increasing NG to 600 does not provide significant improvement of ER for the cascaded configuration, we chose NG $= 400$ to make the device compact. We have derived a FoM parameter from the ER, 3-dB BW and footprint to determine the value of ΔW and ΔL. The FoM has been defined as follows (4): (a) the cascaded configuration footprint is considered as the standard. The footprint of both configurations is divided by the footprint of the cascaded configuration; this is designated as the footprint ratio (FR), (b) the FR is multiplied with the 3-dB BW, and (c) the ER is divided by this product.

$$FoM = \frac{ER}{BW(3dB) \times FR} \tag{4}$$

The FoMs for the single-stage and the cascaded configuration as a function of ΔL for different values of ΔW are presented in Fig. 4. It can be seen that the highest value of FoM for the single-stage and the cascaded configurations are 7.54 dB/nm and 13.83 dB/nm, respectively which occurs at $\Delta W = 80$ nm and $\Delta L = 128$ nm. Therefore, we have used these values for our fabrication.

In order to evaluate the effectiveness of misaligned sidewall Bragg gratings compared to typical aligned sidewall gratings, we study the effect of increasing ΔL versus decreasing ΔW on the coupling coefficients. The coupling coefficients of the BGs for different ΔW with ΔL fixed at zero, and with the ΔW constant at 80 nm for different ΔL were also calculated and are presented in Fig. 5.

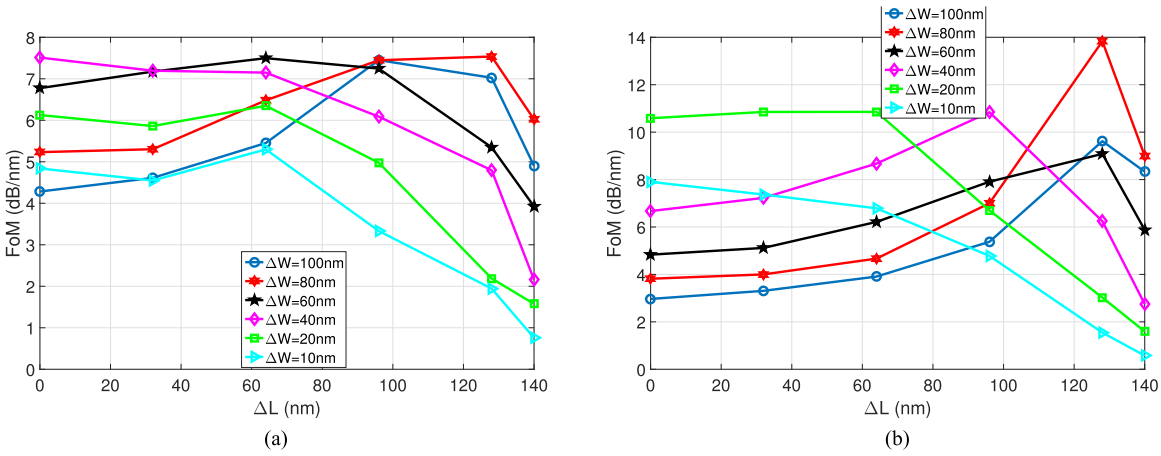

Fig. 4. Figure of merit as a function of ΔL for different ΔW with NG = 400 for the (a) single-stage and the (b) cascaded configuration.

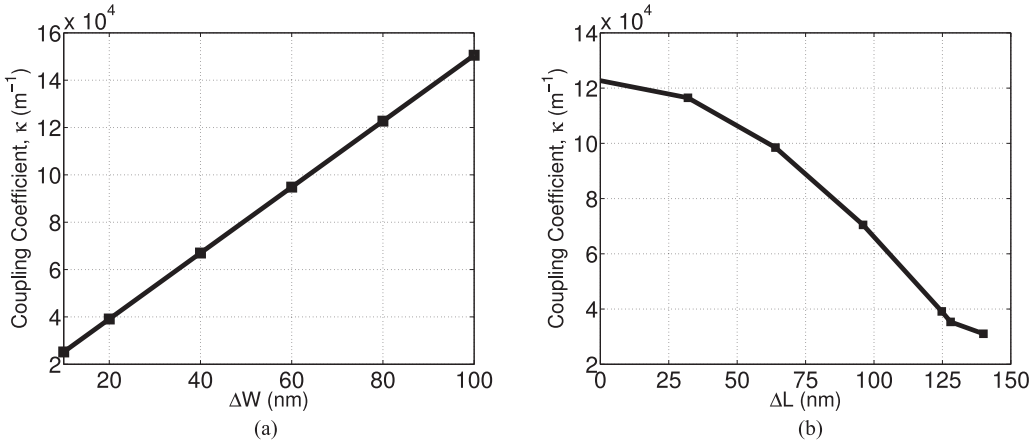

Fig. 5. Simulated coupling coefficients for (a) different ΔW with ΔL = 0 nm, and (b) different ΔL with ΔW = 80 nm.

As can be seen in Fig. 5, the coupling coefficient decreases as ΔW is reduced or ΔL is increased. In terms of practical implementations, varying ΔL to achieve different coupling coefficients is more resistant to fabrication errors as shown in [24]. This can also be attributed to the fact that fabricating small feature size is difficult. For example, from Fig. 5, it can be seen that a coupling coefficient of 3.9×10^4 m^{-1} is obtained at ΔW = 20 nm with ΔL = 0 nm (Fig. 5(a)) which can also be obtained with ΔW = 80 nm and ΔL = 124.7 nm (Fig. 5(b)). The 80 nm feature size will resolve better during fabrication compared to the 20 nm features. The larger ΔW also allowed us to use a smaller number of grating periods and reduce the device footprint.

3. Experimental Results and Discussion

The devices were fabricated with a single-etch process using electron beam lithography [29]. The waveguides have a 500 nm $\times$ 220 nm cross-section with a 3 μm buried oxide and native oxide cladding. Fully-etched sub-wavelength grating couplers were used for coupling light in and out of the OADMs [30]. Calibration grating coupler pairs, with one input grating coupler and one output grating coupler, were used to calibrate the insertion losses of the grating couplers from the test structures. The scanning electron microscope (SEM) images of the fabricated OADMs and misaligned BG with ΔL = 128 nm and ΔW = 80 nm are shown in Fig. 6. Transmission spectra were measured by

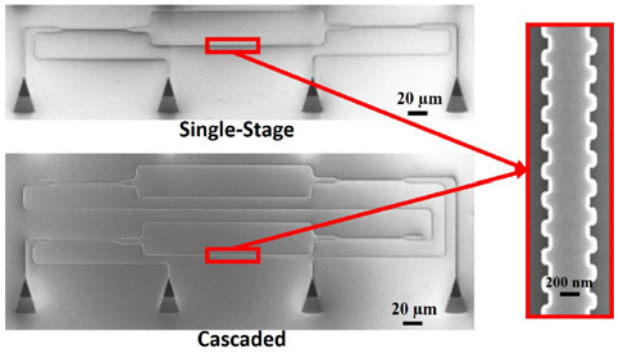

Fig. 6. SEM images of the fabricated single-stage and cascaded OADMs and misaligned sidewall bragg grating with $\Delta L = 128$ nm and $\Delta W = 80$ nm.

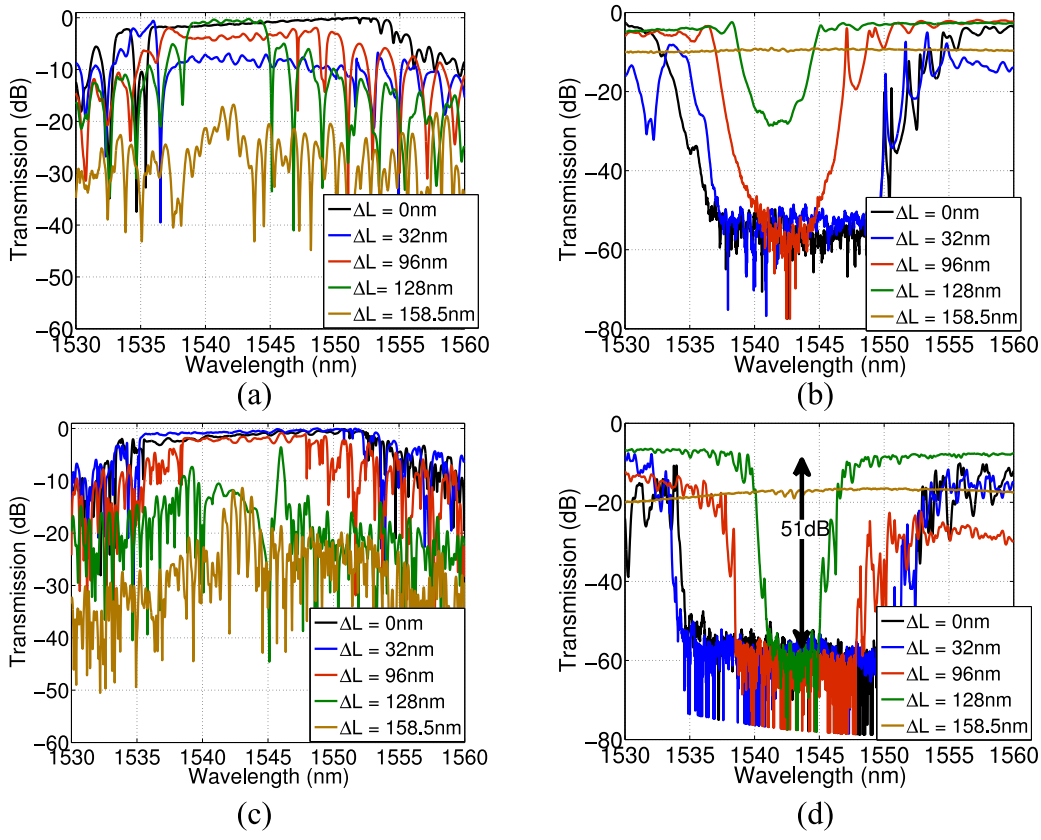

Fig. 7. Measured transmission response of (a) drop and (b) through port of the single-stage configuration, and (c) drop and (d) through port of the cascaded configuration.

sweeping an external cavity laser over the wavelength of interest and recording the output power from various ports of the device with a power meter. The results for both the single-stage and cascaded configurations are presented in Fig. 7. ΔL was varied from 0 nm to half of the grating period, Λ. As can be seen from Fig. 7, for both configurations, the BW reduces as ΔL is increased. This occurs because the reflection from each grating period interferes less constructively as the grating misalignment increases. In case of the single-stage configuration, the ER remains almost constant at 51 dB for up to $\Delta L = 96$ nm and decreases to 25 dB at $\Delta L = 128$ nm. For the case of the cascaded configuration, the ER remains constant at around 51 dB until $\Delta L = 128$ nm. This can be explained from the fact that the cascaded configuration has an intermediate BG, which reflects the

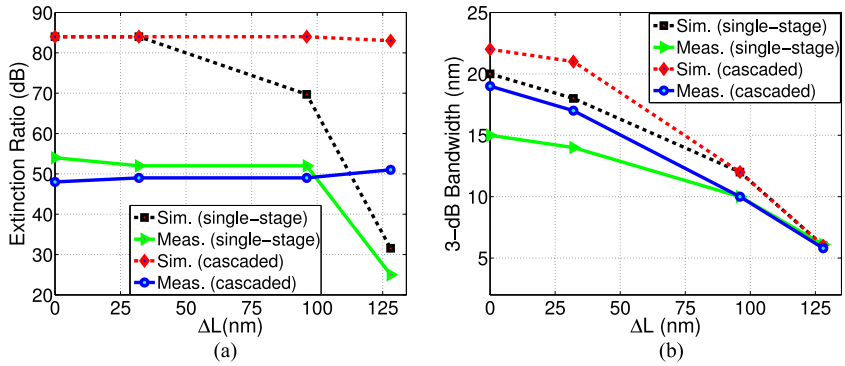

Fig. 8. Comparison for the single-stage and cascaded configurations of the OADMs between the simulated and measured (a) ER, and (b) 3-dB BW. Sim. = Simulated and Meas. = Measured.

residue light that leaks from the first BG, thus achieving a higher ER even at $\Delta L = 128$ nm. At $\Delta L = 158.5$ nm, there is no reflection as demonstrated by the solid brown line in the input-to-through plot of Fig. 7. The measured insertion losses from the input-to-drop port and the input-to-through port are 2 dB and 4.1 dB for the single-stage configuration, and 2 dB and 8.5 dB for the cascaded configuration, respectively. The additional loss in the through port of the cascaded configuration emerges because of the extra path and BGs that the light needs to travel to reach the through port compared to the single-stage configuration. Part of the light also leaks through the add port which is another reason for the increased insertion loss at the through port.

Achieving a high ER is required to reduce the intra-channel crosstalk since it defines the amount of isolation between the add and drop channels. In experiments with high data rate, $<$1 dB penalty can be achieved if a ER of greater than 30 dB is obtained [31]. On the other hand, components with smaller footprints and lower insertion losses are required to satisfy the constraints of integrated optical devices.

The simulated and measured ERs and 3-dB BWs are compared in Fig. 8. Regarding the ER, the difference between the simulated and measured results is large as observed in Fig. 8(a). This is attributed to the -80 dBm sensitivity limit of the power meter used in the experiment. The fact that the ER remains constant with the increase in ΔL (even at 128 nm for the cascaded configuration) provides further evidence that the devices have higher ER than measurable with our equipment. Another evidence is that the simulated and measured ER start to agree for $\Delta L >$100 nm when the simulated ER become $<$50 dB which is within the sensitivity capabilities of the power meter used in the experiment. For the 3-dB BW parameter, the agreement between simulation and measurements is very good and the deviation between the simulated and measured value decreases as ΔL is increased.

Table 1 compares the ER, 3-dB BW, device footprint, and insertion loss of our device with other published works on OADMs in SOI. We have modified the FoM parameter, defined in (4) to include the effect of insertion losses of the devices being compared. The FoM defined in (4) has been divided by the insertion losses of the drop and through ports which resulted in the following equation.

$$FoM_{\text{mod}} = \frac{ER}{BW(3dB) \times FR \times IL_{drop} \times IL_{through}} \tag{5}$$

The footprint of the proposed cascaded configuration is used as the common denominator in determining the footprint ratio of all the devices. In some references, the footprint of the device was not specified and therefore, we were unable to calculate the FoM. In cases where the OADM is multi-channel, we first divided the footprint of that device by the number of channels and then calculated the FoM as mentioned above. A higher value of the FoM is desired since the higher the ER and the smaller the BW, insertion loss and the footprint, the better is the performance of the OADM.

TABLE 1
Comparison With Other Works (ER: Extinction Ratio, *dr*: Input-to-Drop Port, and *th*: Input-to-Through Port.)

	ER (dB)	3-dB BW (nm)	Footprint	Insertion Loss (dB)	FOM_{mod} (/dB-nm)
This work (single-stage)	25	6.2	400 μm $\times$ 90 μm	$dr = 2$ and $th = 4.1$	0.683
This work (cascaded)	51	6	400 μm $\times$ 125 μm	$dr = 2$ and $th = 8.5$	0.500
Wang *et al.* [15]	45	3.5	391 μm $\times$ 3600 μm	$dr = 5$ and $th = 13$	0.007
Naghdi *et al.*[18]	32	3	400 μm $\times$ 90 μm	$dr = 1.2$ and $th = 2$	6.172
Caverly *et al.* [16]	22	4.5	not mentioned	not mentioned	N/A
Yamada *et al.* [19]	8	0.7	800 μm $\times$ 400 μm	$dr = 6$ and $th = 4$	0.074
Qiu *et al.* [17]	5.8	0.8	not mentioned	$dr = 1.6$ and $th = 0.2$	N/A
Wu *et al.* [12]	28.72	1.34	3000 μm $\times$ 500 μm	$dr = 9.94$ and $th = 7.35$	0.039
Yan *et al.* [32]	18	0.15	not mentioned	$dr = 14$ and $th = 12$	N/A
Wu *et al.* [33]	15.74	2	1000 μm $\times$ 760 μm	$dr = 10.52$ and $th = 15.31$	0.026

From Table 1, it can be observed that our cascaded configuration has the highest ER reported thus far for the SOI platform. The input-to-drop and input-to-through insertion losses are also smaller compared to results reported by others. In terms of FoM, both of our designs outperform others significantly, except for the device proposed by Naghdi *et al.* [18] which has better FoM than ours. However, the design proposed by Naghdi *et al.* uses sub-wavelength gratings which are very sensitive to fabrication errors and cannot be fabricated using the large-scale 193 nm deep ultraviolet lithography process. Whereas we have used sidewall Bragg gratings with CMOS compatible feature size which have already been fabricated using deep ultraviolet lithography [34]. In future designs, the sidelobes can be reduced by apodizing the gratings [35]. The misalignment technique to vary the grating strength profile for apodization is more resilient to fabrication errors compared to changing the corrugation amplitude to vary the grating strength profile [24]. Thus, our proposed designs not only provide good performance but also relax fabrication tolerances.

4. Conclusion

We present two configurations of OADM utilizing misaligned sidewall BGs and obtained ERs of 25 dB and 51 dB with a footprint of only 400 μm $\times$ 90 μm and 400 μm $\times$ 125 μm, respectively. We achieved 15 and 28 times less footprint for the single-stage and cascaded OADM respectively and about 3 dB less insertion loss compared to previous BG based OADMs reported in the literature [15]. The feature size used in the designs can be fabricated using 193 nm deep ultraviolet lithography.

Acknowledgment

The authors wish to thank CMC Microsystems, NSERC CREATE Si-EPIC program and Prof. Lukas Chrostowski's group at the University of British Columbia. The devices were fabricated at the University of Washington, Washington Nanofabrication Facility (WNF).

References

[1] D. Thomson *et al.*, "Roadmap on silicon photonics," *J. Opt.*, vol. 18, no. 7, 2016, Art. no. 073003.

[2] D. Liang and J. Bowers, "Photonic integration: Si or InP substrates?" *Electron. Lett.*, vol. 45, no. 12, pp. 578–581, 2009.
[3] B. Milivojevic *et al.*, "112gb/s dp-qpsk transmission over 2427 km ssmf using small-size silicon photonic iq modulator and low-power cmos driver," in *Proc. Opt. Fiber Commun. Conf.*, 2013, Paper OTh1D–1.
[4] H. Yi, Q. Long, W. Tan, L. Li, X. Wang, and Z. Zhou, "Demonstration of low power penalty of silicon Mach–Zehnder modulator in long-haul transmission," *Opt. Exp.*, vol. 20, no. 25, pp. 27 562–27 568, 2012.
[5] C. R. Doerr *et al.*, "Single-chip silicon photonics 100-gb/s coherent transceiver," in *Proc. Opt. Fiber Commun. Conf.*, 2014, Paper Th5C-1.
[6] L. Chen *et al.*, "Silicon photonics for 100g-and-beyond coherent transmissions," in *Proc. Opt. Fiber Commun. Conf. Exhib.,* 2016, pp. 1–3.
[7] S. T. Chu, B. E. Little, W. Pan, T. Kaneko, S. Sato, and Y. Kokubun, "An eight-channel add-drop filter using vertically coupled microring resonators over a cross grid," *IEEE Photon. Technol. Lett.*, vol. 11, no. 6, pp. 691–693, Jun. 1999.
[8] K. Kintaka, J. Nishii, S. Murata, and S. Ura, "Eight-channel wdm intraboard optical interconnect device by integration of add/drop multiplexers in thin-film waveguide," *J. Lightw. Technol.*, vol. 28, no. 9, pp. 1398–1403, May 2010.
[9] B. Little *et al.*, "Very high-order microring resonator filters for wdm applications," *IEEE Photon. Technol. Lett.*, vol. 16, no. 10, pp. 2263–2265, Oct. 2004.
[10] C. R. Giles and M. Spector, "The wavelength add/drop multiplexer for lightwave communication networks," *Bell Labs Tech. J.*, vol. 4, no. 1, pp. 207–229, 1999.
[11] Y. Chen *et al.*, "Low-crosstalk and compact optical add-drop multiplexer using a multiport circulator and fiber Bragg gratings," *IEEE Photon. Technol. Lett.*, vol. 12, no. 10, pp. 1394–1396, Oct. 2000.
[12] D. Wu, Y. Wu, Y. Wang, J. An, and X. Hu, "Four-channel optical add-drop multiplexer based on dual racetrack micro-ring resonators," *Opt. Commun.*, vol. 354, pp. 386–391, 2015.
[13] L. Yangyang, T. Yonghui, and Y. Lin, "Integrated reconfigurable optical add-drop multiplexers based on cascaded microring resonators," *J. Semicond.*, vol. 34, no. 9, 2013, Art. no. 094012.
[14] A. Vorckel, M. Monster, W. Henschel, P. H. Bolivar, and H. Kurz, "Asymmetrically coupled silicon-on-insulator microring resonators for compact add-drop multiplexers," *IEEE Photon. Technol. Lett.*, vol. 15, no. 7, pp. 921–923, Jul. 2003.
[15] J. Wang and L. R. Chen, "Low crosstalk Bragg grating/Mach-Zehnder interferometer optical add-drop multiplexer in silicon photonics," *Opt. Exp.*, vol. 23, no. 20, pp. 26 450–26 459, 2015.
[16] M. Caverley, R. Boeck, L. Chrostowski, and N. A. Jaeger, "High-speed data transmission through silicon contra-directional grating coupler optical add-drop multiplexers," in *Proc. CLEO, QELS_Fundam. Sci.*, 2015, Paper JTh2A-41.
[17] H. Qiu *et al.*, "FSR-free add–drop filter based on silicon grating-assisted contradirectional couplers," *Opt. Lett.*, vol. 38, no. 1, pp. 1–3, 2013.
[18] B. Naghdi and L. R. Chen, "Silicon photonic contradirectional couplers using subwavelength grating waveguides," *Opt. Exp.*, vol. 24, no. 20, pp. 23 429–23 438, 2016.
[19] H. Yamada, T. Chu, S. Ishida, and Y. Arakawa, "Optical add-drop multiplexers based on si-wire waveguides," *Appl. Phys. Lett.*, vol. 86, no. 19, 2005, Art. no. 191107.
[20] W. Shi *et al.*, "Ultra-compact, flat-top demultiplexer using anti-reflection contra-directional couplers for CWDM networks on silicon," *Opt. Exp.*, vol. 21, no. 6, pp. 6733–6738, 2013.
[21] K. Mitsuya, Y. Shoji, and T. Mizumoto, "Demonstration of a silicon waveguide optical circulator," *IEEE Photon. Technol. Lett.*, vol. 25, no. 8, pp. 721–723, Apr. 2013.
[22] S. Ghosh, S. Keyvaninia, W. Van Roy, T. Mizumoto, G. Roelkens, and R. Baets, "Adhesively bonded ce: Yig/soi integrated optical circulator," *Opt. Lett.*, vol. 38, no. 6, pp. 965–967, 2013.
[23] T. Mizuochi, T. Kitayama, K. Shimizu, and K. Ito, "Interferometric crosstalk-free optical add/drop multiplexer using Mach-Zehnder-based fiber gratings," *J. Lightw. Technol.*, vol. 16, no. 2, pp. 265–276, Feb. 1998.
[24] X. Wang *et al.*, "Precise control of the coupling coefficient through destructive interference in silicon waveguide Bragg gratings," *Opt. Lett.*, vol. 39, no. 19, pp. 5519–5522, 2014.
[25] G. T. Reed, *Silicon Photonics: The State of the Art*. New York, NY, USA: Wiley, 2008.
[26] Z. Lu, D. Celo, P. Dumais, E. Bernier, and L. Chrostowski, "Comparison of photonic 2× 2 3-db couplers for 220 nm silicon-on-insulator platforms," in *Proc. 2015 IEEE 12th Int. Conf. Group IV Photon.*, 2015, pp. 57–58.
[27] Lumerical interconnect. 2017. [Online]. Available: https://www.lumerical.com/tcad-products/interconnect/
[28] Si-epic ebeam pdk. 2017. [Online]. Available: https://github.com/lukasc-ubc/SiEPIC_EBeam_PDK
[29] R. J. Bojko, J. Li, L. He, T. Baehr-Jones, M. Hochberg, and Y. Aida, "Electron beam lithography writing strategies for low loss, high confinement silicon optical waveguides," *J. Vac. Sci. Technol. B, Nanotechnol. Microelectron., Mater. Process. Meas. Phenom.*, vol. 29, no. 6, 2011, Art. no. 06F309.
[30] Y. Wang *et al.*, "Focusing sub-wavelength grating couplers with low back reflections for rapid prototyping of silicon photonic circuits," *Opt. Exp.*, vol. 22, no. 17, pp. 20 652–20 662, 2014.
[31] R. J. S. Pedersen and B. Jorgensen, "Impact of coherent crosstalk on usable bandwidth of a grating-MZI based OADM," *IEEE Photon. Technol. Lett.*, vol. 10, no. 4, pp. 558–560, Apr. 1998.
[32] H. Yan, X. Feng, D. Zhang, K. Cui, F. Liu, and Y. Huang, "Compact optical add-drop multiplexers with parent-sub ring resonators on SOI substrates," *IEEE Photon. Technol. Lett.*, vol. 25, no. 15, pp. 1462–1465, Aug. 2013.
[33] D. Wu, Y. Wu, Y. Wang, J. An, and X. Hu, "Reconfigurable optical add-drop multiplexer based on thermally tunable micro-ring resonators," *Opt. Commun.*, vol. 367, pp. 44–49, 2016.
[34] J. St-Yves, S. LaRochelle, and W. Shi, "O-band silicon photonic Bragg-grating multiplexers using uv lithography," in *Proc. Opt. Fiber Commun. Conf.*, 2016, Paper Tu2F–7.
[35] A. D. Simard, N. Belhadj, Y. Painchaud, and S. LaRochelle, "Apodized silicon-on-insulator Bragg gratings," *IEEE Photon. Technol. Lett.*, vol. 24, no. 12, pp. 1033–1035, Jun. 2012.